

**Please cite the Published Version**

Tabar, Fatemeh Ahmadi , Lowdon, Joseph W, Frigoli, Margaux , Crapnell, Robert D , Cleij, Thomas J , Diliën, Hanne, Banks, Craig E , Eersels, Kasper , van Grinsven, Bart  and Wagner, Patrick  (2025) Tracking Perfluorooctanoic Acid in Tap and River Water Employing Screen-Printed Electrodes Modified with Molecularly Imprinted Polymers. ACS Omega, 10 (15). pp. 15018-15028. ISSN 2470-1343

**DOI:** <https://doi.org/10.1021/acsomega.4c10473>

**Publisher:** American Chemical Society (ACS)

**Version:** Published Version

**Downloaded from:** <https://e-space.mmu.ac.uk/639614/>

**Usage rights:**  Creative Commons: Attribution-Noncommercial-No Derivative Works 4.0

**Additional Information:** This is an open access article which first appeared in ACS Omega, published by the American Chemical Society

**Enquiries:**

If you have questions about this document, contact [openresearch@mmu.ac.uk](mailto:openresearch@mmu.ac.uk). Please include the URL of the record in e-space. If you believe that your, or a third party's rights have been compromised through this document please see our Take Down policy (available from <https://www.mmu.ac.uk/library/using-the-library/policies-and-guidelines>)

# Tracking Perfluorooctanoic Acid in Tap and River Water Employing Screen-Printed Electrodes Modified with Molecularly Imprinted Polymers

Fatemeh Ahmadi Tabar,\* Joseph W. Lowdon, Margaux Frigoli, Robert D. Crapnell, Thomas J. Cleij, Hanne Diliën, Craig E. Banks, Kasper Eersels, Bart van Grinsven, and Patrick Wagner\*



Cite This: *ACS Omega* 2025, 10, 15018–15028



Read Online

ACCESS |



Metrics & More

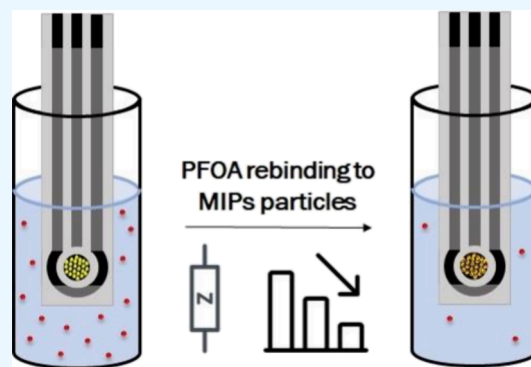


Article Recommendations



Supporting Information

**ABSTRACT:** While existing polyfluoroalkyl substances (PFAS) detection techniques are highly sensitive, their broader implementation is limited by the need for expensive equipment, lengthy analysis times, and specialized personnel. This underscores the need for fast, reliable, cost-effective, and accessible PFAS detection methods to avoid exposure to these pollutants and expedite the remediation of contaminated environments. Currently, portable electrochemical sensors for *in situ* contaminant detection are gaining significant attention. This study focuses on developing an electrochemical sensor for on-site perfluorooctanoic acid (PFOA) detection utilizing screen-printed electrodes (SPEs) modified with molecularly imprinted polymers (MIPs). The sensor's performance is evaluated using electrochemical impedance spectroscopy (EIS), with the electrochemical signals for PFOA detection arising from the specific interactions between MIPs and PFOA. The sensor exhibits a linear response to PFOA in phosphate-buffered saline within a concentration range of 0.1 nM to 10  $\mu$ M, a detection limit of  $19 \pm 1$  pM, and a quantification limit of  $42 \pm 3$  nM. The selectivity of the sensor is assessed by measuring its response to four different PFAS compounds. Additionally, its real-world applicability is tested by analyzing the EIS response in tap and river water samples. The developed sensor, which combines an easy-to-use dipstick format with readily prepared SPEs, has the potential for large-scale production for *in situ* PFOA detection.



## 1. INTRODUCTION

Polyfluoroalkyl substances (PFAS) are a group of widespread and persistent pollutants commonly known as “forever chemicals”. These chemicals are present in a range of consumer goods from cookware and stain-resistant coatings to firefighting foams.<sup>1–3</sup> Their extensive use results in the contamination of air, surface water, groundwater, and soil.<sup>4</sup> Due to the strong carbon-fluoride bonds in PFAS, these chemicals do not decompose in the environment and can eventually contaminate food and drinking water.<sup>5,6</sup> Ingesting contaminated drinking water is a primary route of human exposure to PFAS.<sup>7</sup> The extraordinary chemical stability of PFAS compounds, coupled with their association with adverse health effects such as female infertility, thyroid disease, and cancer, raises significant health concerns.<sup>8–10</sup> Consequently, governmental bodies have implemented widespread regulatory and legal measures to control PFAS use and exposure. For instance, the European Commission (EC) has set maximum contaminant levels in the 2020 EU Drinking Water Directive, limiting each individual PFAS molecule to 0.1  $\mu$ g/L and the total concentration of all PFAS compounds to 0.5  $\mu$ g/L.<sup>11</sup>

Current methods for detecting PFAS typically involve collecting samples and transporting them to analytical

laboratories.<sup>12,13</sup> In these settings, chromatographic and mass spectrometric techniques are employed for the determination and quantification of PFAS.<sup>14–16</sup> Although these methods are highly sensitive and capable of multiplexing, they are expensive and time-consuming and require skilled personnel. This limits their use for routinely screening and early detection of contamination.<sup>17,18</sup> Additionally, environmental factors during transportation can cause variations in PFAS concentrations.<sup>19</sup> Therefore, there is a critical need to develop *in situ*, fast, ultrasensitive, and cost-effective detection techniques to facilitate routine screening and effectively address PFAS pollution.<sup>20,21</sup>

Electrochemical sensors have shown great potential for the fast, cost-effective, and portable detection of a wide range of targets. These systems measure analyte concentrations through

Received: November 18, 2024

Revised: April 2, 2025

Accepted: April 7, 2025

Published: April 12, 2025



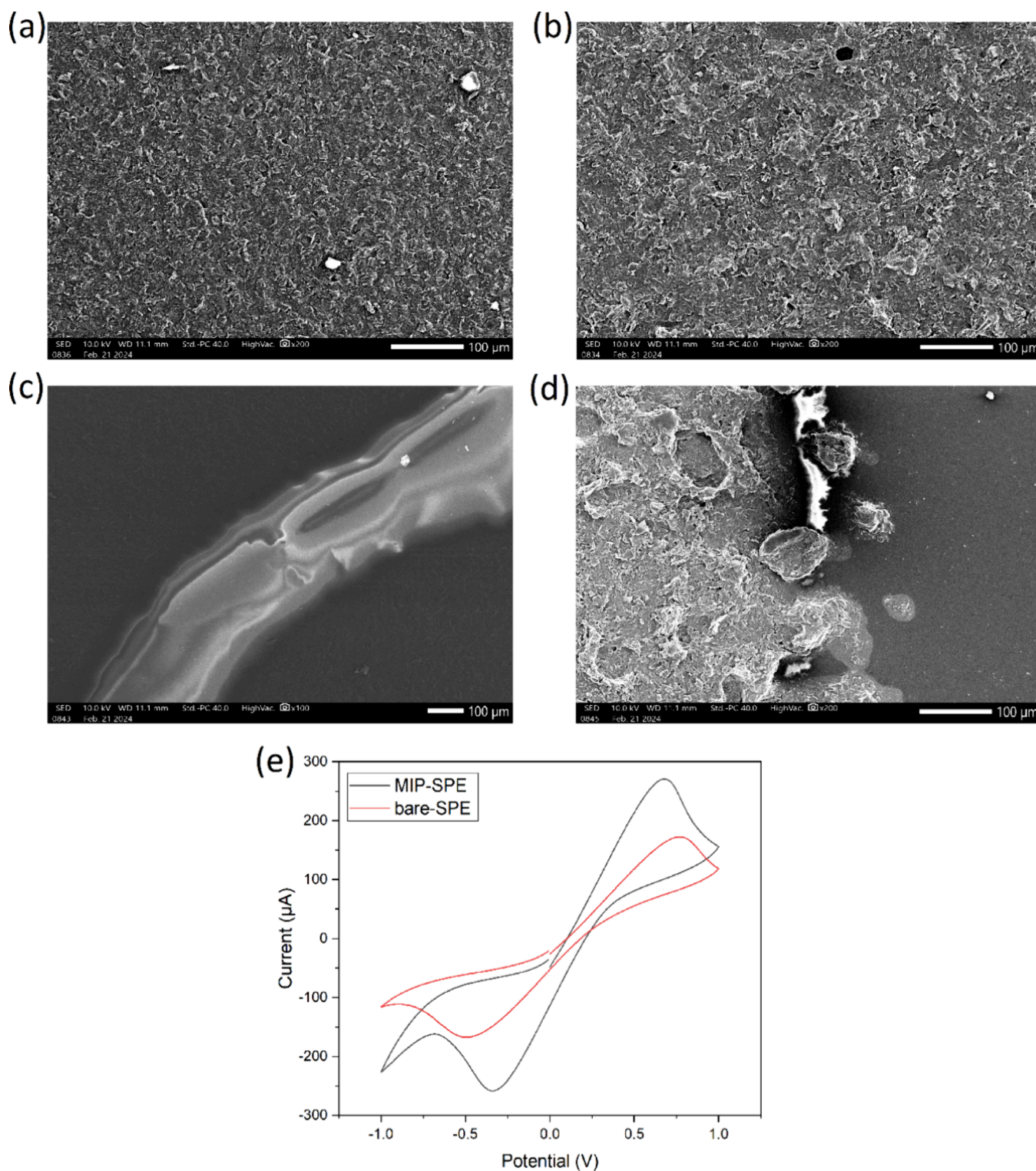


**Figure 1.** Scanning electron microscopy (SEM) images for screen-printed electrodes of (a) unmodified and (b) modified with MIPs (MIP-SPE). SEM images of the electrode edges for (c) bare SPE and (d) MIP-SPE. Scale bars are 100  $\mu\text{m}$ . (e) CV curves of bare SPE and MIP-modified SPE over the potential range of  $-1.0$  to  $1.0$  V and a scan rate of  $0.32$  V  $\text{s}^{-1}$ .

proportional changes in electrochemical responses, such as voltammetric, amperometric, and impedimetric signals.<sup>22</sup> However, the chemical inertness of PFAS presents a significant challenge for direct electrochemical analysis, which relies on selective interactions of target molecules with the electrode surface. To overcome this limitation, a surface functionalization approach is necessary to enable the selective capture of the

target analyte prior to electrochemical detection.<sup>23</sup> Molecularly imprinted polymers (MIPs) can be employed for surface functionalization, enhancing the selectivity of electrochemical sensors and providing a promising platform for the detection of redox-inactive molecules.<sup>24–26</sup>

MIPs are valued for their low cost, excellent chemical and thermal stability, high selectivity, and ability to recognize

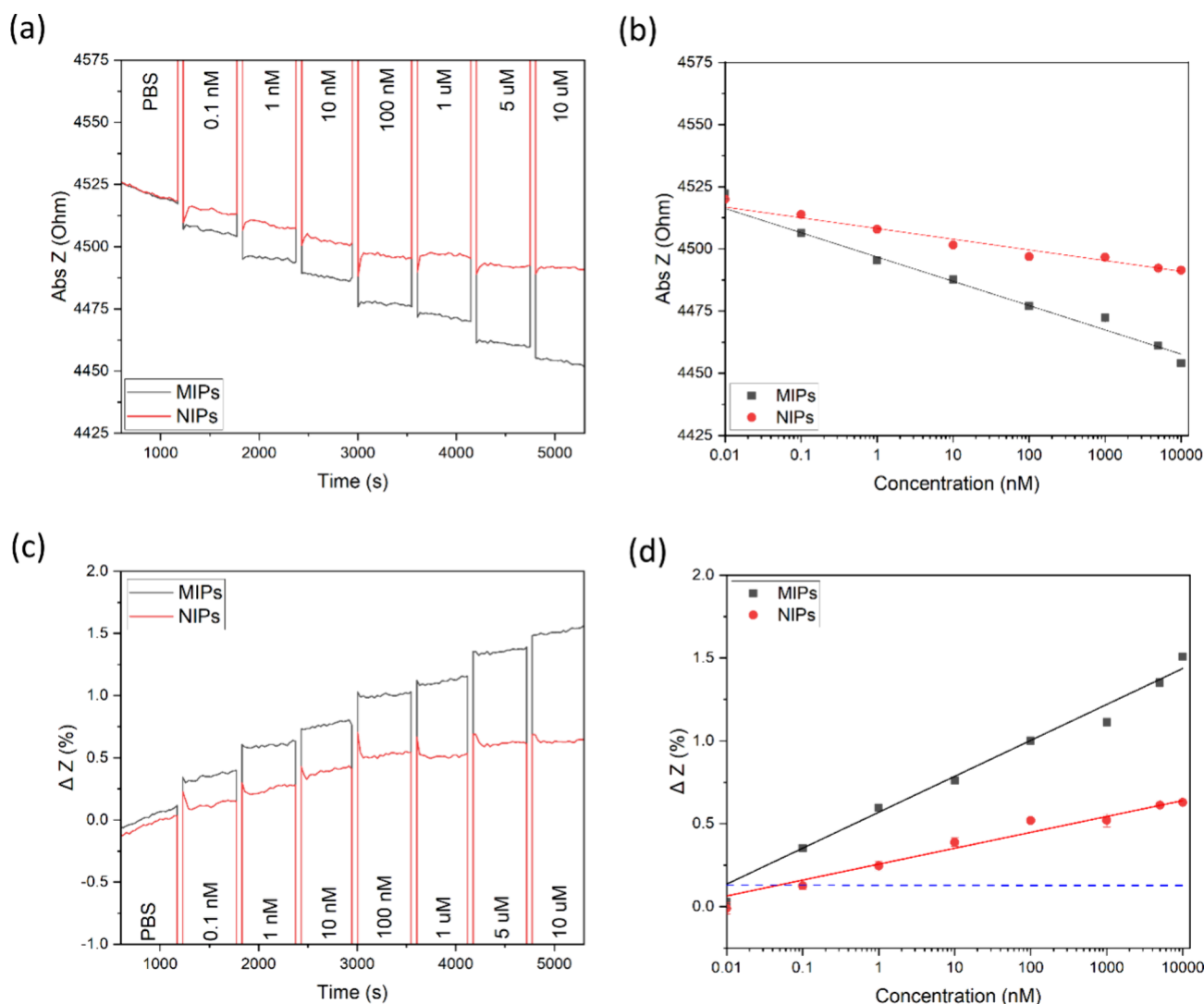


**Figure 2.** Results of EIS rebinding analysis after infusion with different concentrations of PFOA (0.1 nM to 10  $\mu$ M) in PBS. (a) Absolute Z values against time and (b) corresponding dose–response curves for the MIP/NIP modified SPE. (c) Absolute Z value changes against time and (d) corresponding dose–response curves of MIP/NIP modified SPE. The dashed blue line shows the detection limit, determined by the three-sigma rule.

specific target analytes.<sup>27–30</sup> They can be prepared by using various methods, such as precipitation, bulk, and emulsion polymerization. Among these, bulk free radical polymerization stands out as the most straightforward and cost-effective approach for producing large quantities of MIPs.<sup>31–34</sup>

Generally, MIPs are synthesized in the presence of template molecules. After the templates are removed, nanocavities remain within the polymeric substrate.<sup>35–37</sup> These cavities are designed to be complementary to the target molecules in size, shape, and orientation of functional groups.<sup>38,39</sup> Therefore, we have chosen for an affinity-based electrochemical sensor where target detection consists of two crucial phases: (i) the recognition stage, where MIPs capture the target from a sample matrix through specific affinity interactions; and (ii) the transduction stage, which converts these binding events into distinct and quantifiable electrochemical signals.<sup>40,41</sup>

Previously, we coupled MIPs with the heat transfer method to detect perfluorooctanoic acid (PFOA) in environmental samples, recognizing PFOA as one of the most prevalent and harmful components of the PFAS category.<sup>42</sup> The polymer was synthesized via bulk free radical polymerization in the presence

of PFOA as the template analyte. Although this approach has shown promise, it faced challenges in mass-producing the electrodes and miniaturizing the thermal transducer.

In the present study, we leverage these MIPs to modify screen-printed electrodes (SPE), which are suitable for mass production, and quantify PFOA using an electrochemical readout method. Scanning electron microscopy (SEM) and cyclic voltammetry (CV) were conducted on both bare and MIP-modified electrodes to examine their morphologies and surface characteristics. Calibration curves for PFOA in phosphate-buffered saline (PBS) within the concentration range of 0.1 nM to 10  $\mu$ M were generated using electrochemical impedance spectroscopy (EIS), highlighting the difference in detection capabilities between MIP and non-imprinted polymer (NIP) modified electrodes.

The MIP-modified SPE displays a stronger response to PFOA compared to other PFAS molecules, such as perfluorooctanesulfonate (PFOS). Importantly, our findings demonstrate the sensor's applicability in regulatory-relevant matrices, such as tap and river water, yielding highly reproducible results. Impedance analysis revealed optimal

detection limits for PFOA in PBS, tap water, and river water, all below the maximum levels (0.2 nM for PFOA) specified by the EU Drinking Water Directive.<sup>11</sup>

This study presents a significant advancement in MIP-based electrochemical sensing of PFAS, emphasizing simplicity and cost-effectiveness. It also lays the foundation for future research aimed at developing fast, reliable, and portable sensors for PFAS monitoring. To the best of our knowledge, such on-site PFAS sensors are not yet commercially available. Currently, only a few PFAS testing kits exist for field sampling, which require samples to be sent to laboratories for analysis.

## 2. RESULTS AND DISCUSSION

**2.1. Characterization with SEM and CV.** The morphological studies on the functionalized part of the screen-printed electrodes were carried out using scanning electron microscopy (SEM) combined with an energy dispersive X-ray (EDX) detector (Figure 1). Observing the images of the unmodified SPE revealed an inhomogeneous and uneven surface (Figure 1a). In contrast, the microscopy images of the MIP-modified SPE show a distinct pattern (Figure 1b). The modification with polymer particles is evident, as the surface appears to be more porous and rougher.

SEM images were captured from the edges of both the bare and MIP-SPE working electrodes (Figure 1c,d). The presence of some small particles on the edges of MIP-modified SPE highlights its difference with the bare SPE, which has flat and comparatively smooth edges. Notably, a small peak of oxygen is detected in the EDX pattern of the modified-SPE, likely due to the presence of oxygen in polyacrylamide MIPs (Supporting Information Figure S1).

The electrochemical properties of the bare and modified SPEs were assessed by CV with a  $[\text{Fe}(\text{CN})_6]^{3-}/4-$  redox probe in PBS. As shown in Figure 1e, the CV graph of the MIP-modified SPE indicates higher oxidation and reduction peaks compared to the bare SPE. Additionally, the area enclosed by the CV graph of MIP-modified SPE is significantly larger than that of the bare SPE. This can be attributed to the more porous morphology of MIP-modified SPE, which results in more active sites available for redox reactions.

**2.2. EIS Measurements in PBS.** To demonstrate the ability of the MIP-modified SPE substrate to rebind PFOA, EIS experiments were performed in phosphate-buffered saline without using a redox probe. The electrochemical behavior of PFAS under impedance spectroscopy primarily involves interface interactions and charge transfer processes at the electrode surface. PFAS molecules can influence the system's impedance through adsorption effects and changes in double-layer capacitance, and this was monitored throughout the study.<sup>43</sup> For each rebinding test, the electrode's modified part was placed into a vial containing PBS for 20 min to allow the impedance signal to stabilize. The sensor was then immersed in vials with varying concentrations of PFOA (ranging from 0.1 nM to 10  $\mu\text{M}$ ), and the impedance signal was recorded for 10 min at each concentration (Figure S2). The experiments with the NIP-modified SPE were conducted in the same way.

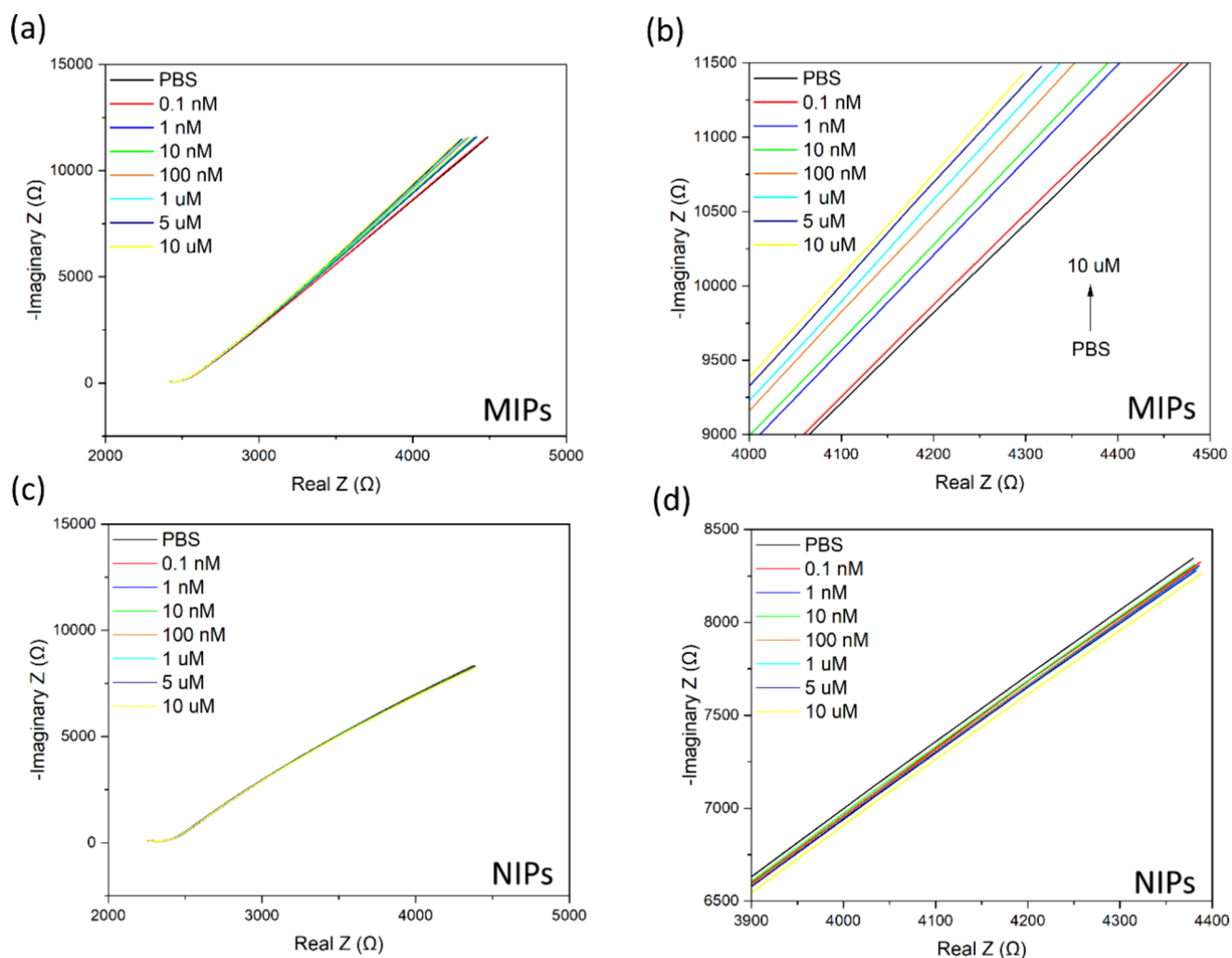
The results reveal that MIP-SPE can specifically bind PFOA, as evidenced by a clear reduction in the absolute impedance value even at very low PFOA concentration (Figure 2a). The NIP-SPE also exhibited a decrease of the impedance value, however much less pronounced in comparison to the MIP-SPE.

The decrease in impedance amplitude upon binding of PFOA by the MIPs can be explained by a scenario in which the lipophilic tail group of PFOA primarily interacts with the molecularly imprinted cavities. In this configuration, the polar head groups are exposed at the interface between the MIP surface and the aqueous sample, increasing the double-layer capacitance by attracting counterions and reorienting water dipoles. This rise in the capacitive contribution directly results in a drop in impedance. Conversely, if the polar head groups bind to the MIP cavities while the lipophilic tails remain exposed to the liquid, the double layer would be disrupted, leading to a decrease in capacitance and an increase in impedance amplitude.<sup>44,45</sup> However, this scenario is not supported by our experimental data and is unlikely due to the incompatibility between the apolar tails and the polar aqueous medium.<sup>46,47</sup>

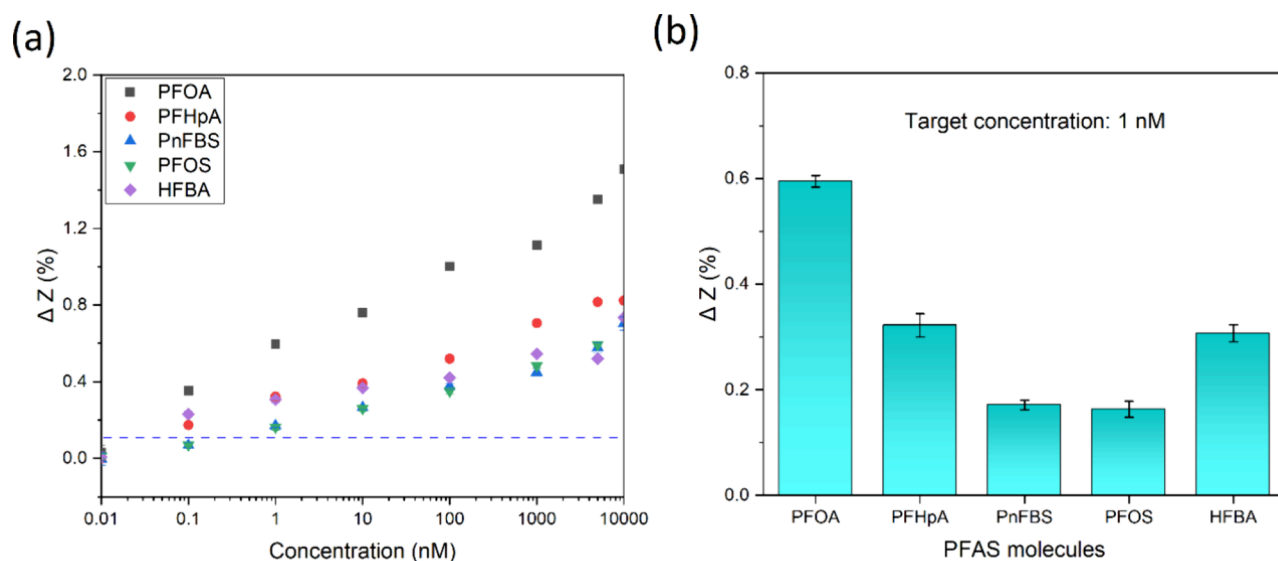
To quantify the impact of different concentrations of PFOA, dose-response curves were generated by plotting the average absolute impedance values over 5 min for each concentration for both MIP-SPE and NIP-SPE (Figure 2b). The error bars for each concentration reflect the variation in absolute impedance values within the 5 min interval. The MIP-SPE displays a linear correlation between impedance values and the logarithm of PFOA concentrations (black line,  $R^2 = 0.97$ ) without saturation effects, indicating the sensor's effectiveness at even higher PFOA concentrations, particularly in PBS samples. Conversely, NIP-SPE shows a diminished and leveling-off response at higher PFOA concentrations (red line,  $R^2 = 0.95$ ). The nonspecific binding of PFOA with the NIP results in much smaller changes in the electrochemical signal across the entire concentration range, highlighting the specificity of the MIP sensor. This specificity underscores the superior performance of the MIP-SPE in detecting PFOA, demonstrating its potential as a reliable and effective tool for monitoring this pollutant.

Figure 2c illustrates the relative impedance changes  $\Delta Z$  (%) over time; these data are normalized with respect to the baseline values in PBS. To accurately determine the sensor's limit-of-detection (LoD), the  $\Delta Z$  (%) data are plotted against the logarithm of PFOA concentration in Figure 2d. The graphs were linearly fitted, demonstrating the sensor's effective range between 0.01 nM and 10  $\mu\text{M}$ . Efforts were then made to establish a practical detection limit, defined by the lowest concentration of PFOA that is reliably analyzable with this setup. Consequently, a limit of detection of 0.1 nM was achieved, which is below the regulatory cutoff values.<sup>11</sup>

The ability to directly detect and quantify a concentration of 0.1 nM highlights a significant improvement over some previously reported electrochemical techniques.<sup>46,47</sup> Furthermore, the theoretical LoD was also calculated as the minimum concentration where the effect size exceeds three times the average noise value across all data sets (dashed blue line, three-sigma rule), resulting in a value of  $19 \pm 1$  pM. Notably, each data point in the data set represents the average of three individual measurements, ensuring reproducibility. The limit of quantification (LoQ) was calculated similarly to the LoD, but instead of multiplying by three times the average noise value, it was multiplied by ten to ensure reliable quantification at higher concentrations, yielding a LoQ of  $42 \pm 3$  nM. Furthermore, % RSD values were calculated based on the variations in absolute impedance changes at each concentration, averaged across three individual SPEs electrodes, with a maximum observed % RSD of 7%.



**Figure 3.** (a, b) Nyquist plots for MIP-modified SPEs at different PFOA concentrations. The plots represent the same data but are shown at different scales to better illustrate the variations in impedance response across different concentrations. (c, d) Nyquist plots for NIP-modified SPEs at different PFOA concentrations.



**Figure 4.** Selectivity results obtained via EIS measurements. (a) Dose–response curves after exposure of MIP-SPE to different concentrations of PFOA, PFHpA, PnFBS, PFOS, and HFBA in PBS. The dashed blue line is representative of the detection limit, determined by the three-sigma rule. (b) MIP-SPE response  $\Delta Z$  (%) after being exposed to 1 nM of different PFAS molecules in PBS. The results are the average of three independent measurements, and the error bars are the standard deviations.

Figure 3 presents the Nyquist plots for MIP/NIP-modified SPEs at varying PFOA concentrations. As the PFOA concentration increases, the slope of the Nyquist plot rises for MIP-SPE, while it remains relatively unchanged for NIP-SPE. These results are consistent with previous data, as the Nyquist plot slope reflects the balance between resistive and capacitive contributions, and the increase in slope suggests that the system is becoming more capacitive, which facilitates charge transfer. This effect is absent in NIP-SPE, where no specific PFOA binding occurs, leading to a relatively unchanged Nyquist plot slope.

The Bode plots for MIP-SPE at different concentrations of PFOA are provided in Supporting Information Figure S3. From the Bode plots, PFOA binding reduces surface roughness by forming a more uniform molecular layer and then the system behaves more like an ideal capacitor, causing the phase angle to shift toward less negative values (closer to  $0^\circ$ ).

**2.3. Selectivity Measurements of MIP-SPE.** When evaluating MIPs as receptors, it is crucial to consider their selectivity toward a specific target over competing molecules. However, in terms of PFAS detection, it is often desirable to detect multiple compounds simultaneously to verify their presence in the same sample. To assess the selectivity of the MIP-modified electrode, the EIS response to other PFAS molecules was studied, as shown in Figure 4. The sensor's response to PFOA is noticeably stronger than that to other PFAS molecules. Two of these tested molecules are HFBA and PFHpA, which share the same functional groups as PFOA (they have a carboxylic acid ( $-\text{COOH}$ ) group attached to a fully fluorinated alkyl chain). Despite this similarity, PFOA has a longer carbon chain and likely a different orientation of the functional groups, which could explain the higher sensor response to PFOA compared to those of HFBA and PFHpA.

The other PFAS molecules, PFOS and PnFBS, have sulfonic acid functional groups. The MIP-SPE sensor also demonstrates a low response toward these two molecules. Therefore, the size, functional groups, and their position can hinder the potential interactions of the PFAS compounds with the MIP-modified surface of the SPE. Figure 4b presents the column graph of MIP-SPE response ( $\Delta Z$  %) after exposure to 1 nM of the mentioned PFAS molecules in PBS.

This selectivity study provides further insight into the binding mechanism of PFOA, shedding light on why a conductive effect is observed rather than a resistive one. The insulating effect of PFAS molecules typically arises from the length of their alkyl tails, where longer tails create a more resistive bilayer that inhibits charge transfer. However, contrary to this norm, our findings reveal the opposite effect, suggesting significant involvement of the alkyl component of PFAS molecules in binding to cavities within the MIP. This enhances our understanding of why increasing PFAS concentrations lead to charge accumulation as the charged head of the PFAS molecule becomes more exposed to the solution.

In summary, the results of these selectivity experiments demonstrate that the sensor reacts more strongly to PFOA but is also capable of recognizing other PFAS species. This is an important finding for future research, as multiplexing the sensor with different PFAS MIPs will enable the accurate determination of both the total PFAS content and the individual contributing compounds in mixed samples.

**2.4. EIS Analysis in Tap and River Water.** The direct application of the developed sensor for detecting PFOA was demonstrated through an EIS analysis of tap water samples

containing the target compound. Initially, an LC-MS instrument was used to assess the tap water and Milli-Q (MQ) water samples for the presence of PFOA. Before spiking, neither MQ water nor tap water showed any detectable PFOA. However, the MQ water sample displayed a distinctive PFOA peak after being spiked with PFOA (see Supporting Information Figure S4). For the rebinding analysis, PBS tablets and various quantities of PFOA were added to the tap water samples without the need for additional treatments. EIS measurements were then performed under the same conditions as for MQ water (with PBS tablets).

From the collected data, a reduction in absolute impedance was observed for the MIP-SPE as PFOA concentrations increased (Supporting Information Figure S5). The normalized responses obtained with both MQ water and tap water are presented in Figure 5. It is evident that the sensor's overall

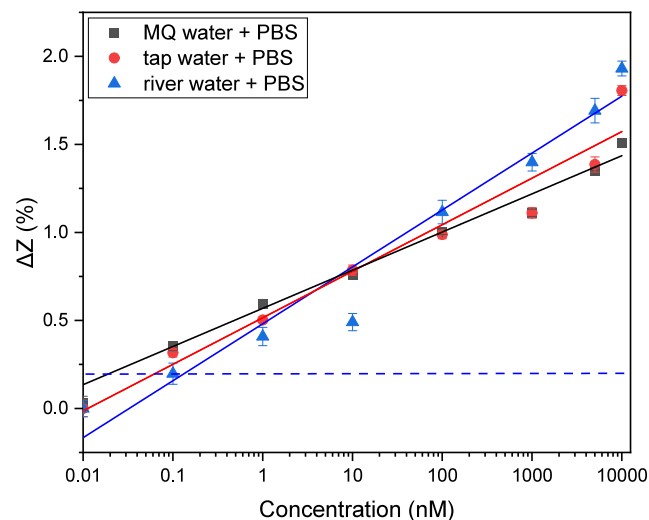


**Figure 5.** EIS rebinding analysis in tap water and river water. Dose–response curves of the  $\Delta Z$  (%) values for MIP-modified SPE in MQ water + PBS, tap water + PBS, and river water + PBS. The graph is obtained from the time-dependent absolute  $Z$  values of MIP-SPE after exposure to increasing concentrations of PFOA. The blue dashed line shows the detection limit established by the three-sigma method. The error bars are the standard deviations. The  $R^2$  values for the fitting graphs were 98% for MQ water, 94% for tap water, and 94% for river water.

response in tap water is very similar to its performance in MQ water. For instance, a significant shift in the absolute impedance values is observed even after exposure of the MIP-modified SPE to very low concentrations of PFOA. Furthermore, the impedance changes display a linear growth when the MIP-SPE is exposed to higher concentrations of PFOA.

This demonstrates that the increased complexity of tap water does not significantly influence the sensor's efficiency, indicating its potential for PFOA detection in various aqueous samples. The LoD was again determined by the three-sigma method, represented by the blue dashed line. The LoD for tap water was calculated to be  $61 \pm 4$  pM, which is comparable to the sensor's LoD in MQ water and meets the requirements of the EU Drinking Water Directive. These findings suggest that the method can be used for quick and inexpensive screening of tap water for PFOA contamination, adhering to the European Council's limit of  $0.1 \mu\text{g/L}$  ( $0.24$  nM) for PFOA.<sup>11</sup>

**Table 1. Comparison of Different Electrochemical Platforms for PFAS Detection in Terms of the Receptor Material, Targeted Analyte, Electrochemical Test Principle, Real-World Samples, and Achieved LoD<sup>a</sup>**

receptor material and electrode type	analyte	electrochemical transducer	water sample	detection	ref.
poly <i>o</i> -PD and gold electrode	PFOS	DPV	tap water	0.04 nM	50
poly <i>o</i> -PD/AuNS & GCE	PFOS	DPV	tap water	0.015 nM	45
poly <i>o</i> -PD & GCE	PFOS	EIS	river water, tap water, lake water	3.4 pM	51
MOFs Cr-MIL-10 and interdigitated microelectrodes	PFOS	EIS	groundwater	1 pM	52
MIP-supported diamond-rich carbon nanoarchitectures and silicon wafer slides	PFOS	DPV and EIS	tap water and wastewater	1.2 $\mu$ g/l (2.4 nM)	47
WS <sub>2</sub> -MWCNT & freestanding electrode	PFOA	CV	tap water	2.404 pM	53
polyaniline-chitosan & SPE	PFOA	CV and DPV	wastewater	1.08 ppb (2.6 nM)	46
fluorine-functionalized Ce-UiO-66 & GCE	PFOA	LSV	river water, tap water, lake water	0.048 nM	54
polyacrylamide & SPE	PFOA	EIS	tap water	19 pM	present study

<sup>a</sup>Abbreviations: *o*-PD: *o*-phenylenediamine; (*o*-PD); DPV: differential pulse voltammetry; AuNS: gold nanostars; GCE: glassy carbon electrode; WS<sub>2</sub>: tungsten disulfide; MWCNTs: multiwalled carbon nanotubes; MOFs Cr-MIL-10: chromium-based metal–organic framework; LSV: linear sweep voltammetry. For better comparability, certain detection limits from the original publications were recalculated to the molar scale; these values are given in brackets.

To further validate the applicability of the developed electrochemical sensor, additional measurements were performed in river water. River water samples were spiked with varying concentrations of PFOA (0.1 nM–10  $\mu$ M). The obtained linear regression for river water closely aligns with those for tap water and MQ water, indicating that the sensor is suitable for detecting PFOA in various real water-based samples. The LoD of the sensor in river water was determined to be  $123 \pm 8$  pM, which is well below the recommended advisory limit.<sup>11</sup>

To evaluate the sensor's performance in real-world conditions, its response to PFOA was tested in the presence of 350 nM caffeine, a common water contaminant.<sup>48</sup> Due to high human consumption, Caffeine is frequently detected in tap and river water.<sup>49</sup> It shares some chemical properties with PFAS and can potentially interfere with sensor readings. Indeed, PFOA and Caffeine both have polar functional groups and hydrophobic regions. The sensor demonstrated a clear response to PFOA even in the presence of caffeine, confirming its robustness for real-sample analysis (see [Supporting Information Figure S6](#) for details).

In summary, an affinity-based sensor was designed by integrating a commercially available SPE covered with PFOA-MIP and an impedance analyzer. This innovative device can be employed as a dipstick sensor for the prompt detection of PFOA in tap water. The sensing process involved immersing the sensor into tap water samples spiked with varying PFOA levels.

To benchmark the sensor's performance, it can now be compared to other electrochemical PFAS sensing platforms reported in the literature. This comparative analysis is presented in [Table 1](#), outlining the receptor material and electrode type, target analyte, used electrochemical transducer principle, real-world sample, and achieved LoD for each study. It is evident from the table that our sensor exhibits a comparatively low detection limit. Furthermore, the developed sensor competes well with other platforms documented in the literature due to its simple and cost-effective detection approach, which eliminates the need for complex data processing.

### 3. CONCLUSIONS

In this study, PFOA-MIP particles were utilized as the receptor material to construct MIP-modified screen-printed electrodes (MIP-SPE) for PFOA detection. The fabrication of MIP-SPE sensors involved a highly reproducible and straightforward process of screen-printing a formulation of MIPs and carbon-graphite ink on the sensing part of an SPE. The results of the EIS rebinding analysis for SPE revealed exceptional sensitivity and acceptable selectivity, enabling the electrochemical quantification of PFOA in PBS. The sensor is able to detect PFOA in a broad range from 0.1 nM to 10  $\mu$ M, and the calculated LoD and LoQ are 19 pM and 42 nM, respectively, while the LoD is below the contaminant level defined by the European Council. Furthermore, the sensor is able to differentiate between different PFAS molecules in PBS. However, PFAS molecules with functional groups similar to those of PFOA exhibited stronger signals compared to the others. The performance of the sensor remained unaffected when it was exposed to tap water and river water as a relevant real-world matrix with LoD values of 61 and 123 pM, respectively. The sensor demonstrated a clear response to PFOA even in the presence of 350 nM caffeine, confirming its robustness for real-sample analysis.

These results demonstrate that the approach adopted in this study is highly promising. The combination of MIPs and SPEs allows for mass-producing large batches of sensor chips, while the integration with EIS and a SPE cartridge allows for the development of a hand-held sensor that can eventually be used also by nonexperienced individuals. Future research should be aimed at investigating how the sensor can be used for the simultaneous and selective detection of different PFAS molecules. Additionally, the sensor's specificity and selectivity can be evaluated across various pH ranges and in the presence of different interferents.

### 4. MATERIALS AND METHODS

**4.1. Materials.** Ethylene glycol dimethacrylate (EGDMA,  $\geq 98\%$ ), azobis(isobutyronitrile) (AIBN,  $\geq 98\%$ ), tridecafluoro-heptanoic acid (PFHpA,  $\geq 97\%$ ), nonafluoro-1-butanefluoric acid potassium salt (PnFBS, 98%), PFOS

(98%), heptafluorobutyric acid (HFBA, 98%), PFOA (95%), acetic acid ( $\geq 99.8\%$ ), and caffeine were supplied by Sigma-Aldrich (The Netherlands). Acrylamide ( $\geq 99.9\%$ ), methanol ( $\geq 99.9\%$ ), and dimethyl sulfoxide (DMSO,  $\geq 99.7\%$ ) were obtained from Fisher Scientific (The Netherlands). The Ag/AgCl and dielectric paste with the product codes of C2040308P3 and D2070423D5 were purchased from Gwent Electronic Materials Ltd., UK. Milli-Q water (resistivity  $\approx 18.1 \text{ M}\Omega \text{ cm}$ ) was used to prepare all test solutions for electrochemical analysis.

#### 4.2. Synthesis of Molecularly Imprinted Polymers.

Molecularly imprinted polymers (MIPs) aimed at detecting PFOA were prepared by using a free-radical bulk polymerization method. The details of the synthesis process have been reported in our previous study.<sup>55</sup> In summary, a mixture of PFOA (0.29 mmol), acrylamide (1.14 mmol), EGDMA (3.46 mmol), and AIBN (0.29 mmol) was prepared in DMSO (3.5 mL). This solution was then subjected to nitrogen purging to remove the undesired gaseous compounds. Following this, the polymerization was initiated at  $65^\circ \text{C}$  for 2 h, and the resulting solid was pulverized and washed with methanol. The template molecule was removed from the imprinted polymer using an extraction method described previously.<sup>55</sup> Finally, the MIPs were dried and ground by using a ball mill machine (at 300 rpm, 180 s, 10 mm balls). Nonimprinted polymers (NIPs) as control were synthesized by the same steps as the MIPs but in the absence of PFOA.

**4.3. Preparation and Modification of the Screen-Printed Electrodes (SPE).** For electrochemical experiments, a microDEK 1760RS screen printer machine (DEK, UK) was employed to fabricate the SPE. For each SPE, a carbon-graphite ink mixture was deposited onto a flexible polyester film with a thickness of  $250 \mu\text{m}$ . This printed layer was then cured at  $60^\circ \text{C}$  for 30 min in a ventilated oven. Subsequently, a reference electrode made of silver/silver chloride (Ag/AgCl, ratio 60:40) was screen printed using Ag/AgCl paste onto the plastic substrate and cured at similar conditions as the previous layer. A dielectric layer of paste was then applied to insulate the connections and determine the 3 mm diameter graphite working electrode. The SPEs were subjected to a final curing step, and then they were ready for use, with their characteristics thoroughly documented in prior studies.<sup>56,57</sup>

To fabricate PFOA-MIP modified screen-printed electrodes (MIP-SPE), the base carbon-graphite ink was modified by incorporating the PFOA-MIP powder. The incorporation process involved calculating the weight percentage of PFOA-MIP particles (MP) to the total ink mass (MI), including both the base ink and the added MIPs, following the formula of  $(\text{MP}/\text{MI}) \times 100$ . The MP was thoroughly mixed with the ink and deposited onto the surface of the working electrode. A formulation of 5 wt % MIP-SPE was selected to ensure there is a sufficient amount of MIP particles on the electrode surface to bind with the target and allow evaluation of the sensor's performance. Additionally, the thickness of the layers of both bare and functionalized SPEs was measured, revealing a value of  $7.03 \pm 1.54 \mu\text{m}$ . It is important to note that the overall thickness of both samples is similar, as the main difference between them is the presence (functionalized) or absence (bare) of MIPs/NIPs particles in the carbon-graphitic ink rather than any differences in the manufacturing process. To assess the stability, electrodes were fabricated using MIPs from different batches produced on separate days and stored for periods ranging from several weeks to months.

**4.4. Characterization of the SPE.** To examine the morphological properties of both the modified and unmodified screen-printed electrodes, they were coated with gold by using a gold-sputtering machine and then imaged with a Scios Dual beam scanning electron microscope at an acceleration voltage of 10 kV and a magnification of  $\times 200$ . Cyclic voltammetry (CV) experiments were conducted via a PalmSens4 potentiostat (PalmSens BV, The Netherlands) to investigate the effect of modification with MIPs particles on the bare SPE. The CV scans were carried out at a potential sweep from  $-1.0$  to  $1.0 \text{ V}$  in an electrolyte solution of  $0.01 \text{ M} [\text{Fe}(\text{CN})_6]^{3-}/4-$ . The scan rate, voltage step, equilibration time, and number of scans were  $0.32 \text{ V s}^{-1}$ ,  $0.01 \text{ V}$ ,  $2 \text{ s}$ , and  $1$ , respectively.

#### 4.5. Electrochemical Impedance Spectroscopy (EIS).

An MFIA impedance analyzer (Zurich Instruments, Switzerland) was employed to perform the EIS analysis on the functionalized SPE at room temperature. The SPEs were connected to the impedance analyzer via a portable SPE connector (PalmSens BV, The Netherlands). Subsequently, the functionalized part of the SPE was immersed into a vial, filled with 5 mL of PFOA solution in PBS, with a concentration range from  $0.1 \text{ nM}$ – $10 \mu\text{M}$ . Continuous frequency sweeps were conducted in the frequency range between  $10 \text{ Hz}$  and  $100 \text{ kHz}$  at a test signal of  $300 \text{ mV}$ . The absolute impedance values at a specific frequency, where the corresponding phase angle reaches  $-45^\circ$ , were used to create the EIS rebinding curves. This frequency varied between different electrodes, but it was always in the range between  $20$  and  $45 \text{ Hz}$ . Table 2 provides an overview of the parameters used for electrochemical measurements, including CV and EIS.

**Table 2. Overview of the Parameters for Electrochemical Measurements**

method	parameter	details
cyclic voltammetry (CV)	instrument	PalmSens4 potentiostat (PalmSens BV, Netherlands)
	electrolyte	$0.01 \text{ M} [\text{Fe}(\text{CN})_6]^{3-}/4-$
	potential range	$-1.0$ to $1.0 \text{ V}$
	scan rate	$0.32 \text{ V/s}$
	voltage step	$0.01 \text{ V}$
	equilibration time	$2 \text{ s}$
	number of scans	$1$
	electrochemical impedance spectroscopy (EIS)	instrument
SPE connection		portable SPE connector (PalmSens BV, Netherlands)
measurement solution		$5 \text{ mL}$ PFOA solution in PBS ( $0.1 \text{ nM}$ – $10 \mu\text{M}$ )
frequency range		$10 \text{ Hz}$ – $100 \text{ kHz}$
test signal		$300 \text{ mV}$
data extraction		absolute impedance at phase angle $-45^\circ$
frequency range for data extraction		$20$ – $45 \text{ Hz}$

All time-dependent impedance analysis results were calculated based on the mean values of three independent, identically performed tests. The  $\Delta Z$  (%) was calculated as the difference between the absolute  $Z$  value and the baseline absolute  $Z$  value after stabilization in PBS ( $Z_{\text{PBS}}$ ), divided by  $Z_{\text{PBS}}$  and then multiplied by  $100$  according to eq 1.

$$\Delta Z(\%) = \frac{Z - Z_{\text{PBS}}}{Z_{\text{PBS}}} \times 100 \quad (1)$$

**4.6. EIS Analysis in Tap and River Water and in the Presence of Caffeine.** Tap water samples were collected from urban sources in Maastricht, The Netherlands, where tap water originates from groundwater or surface water. The absence of PFOA in the samples was verified using a Shimadzu liquid chromatograph–mass spectrometer (LCMS-2020). Subsequently, spiked tap water samples with varying concentrations of PFOA (0.1 nM–10 μM) were generated and utilized for EIS rebinding analysis without additional processing of the samples. In addition, PBS tablets were introduced into the tap water samples to increase their conductivity (one tablet per 100 mL of tap water, 1× PBS). River water samples were taken from the Maas River in Maastricht, The Netherlands, and filtered through a 0.45 μm syringe filter to eliminate insoluble particles. The spiking procedure for river water followed the same steps as those for tap water. For caffeine interference studies, 350 nM caffeine was added to all PFOA concentration series in PBS.

## ■ ASSOCIATED CONTENT

### SI Supporting Information

The Supporting Information is available free of charge at <https://pubs.acs.org/doi/10.1021/acsomega.4c10473>.

EDX patterns of modified SPEs; schematic of MIP-coated dipstick sensor; Bode plots; LC-MS spectra; absolute *Z* values over time for MIP-SPE in tap water; and dose–response curves for MIP-SPE with and without caffeine (PDF)

## ■ AUTHOR INFORMATION

### Corresponding Authors

**Fatemeh Ahmadi Tabar** – Department of Physics and Astronomy, Laboratory for Soft Matter and Biophysics ZMB, KU Leuven, Leuven B-3001, Belgium; Sensor Engineering Department, Faculty of Science and Engineering, Maastricht University, Maastricht 6200 MD, The Netherlands; [orcid.org/0000-0003-1119-0439](https://orcid.org/0000-0003-1119-0439); Email: [fatemeh.ahmaditabar@kuleuven.be](mailto:fatemeh.ahmaditabar@kuleuven.be)

**Patrick Wagner** – Department of Physics and Astronomy, Laboratory for Soft Matter and Biophysics ZMB, KU Leuven, Leuven B-3001, Belgium; [orcid.org/0000-0002-4028-3629](https://orcid.org/0000-0002-4028-3629); Email: [PatrickHermann.Wagner@kuleuven.be](mailto:PatrickHermann.Wagner@kuleuven.be)

### Authors

**Joseph W. Lowdon** – Sensor Engineering Department, Faculty of Science and Engineering, Maastricht University, Maastricht 6200 MD, The Netherlands

**Margaux Frigoli** – Sensor Engineering Department, Faculty of Science and Engineering, Maastricht University, Maastricht 6200 MD, The Netherlands; [orcid.org/0000-0001-8543-741X](https://orcid.org/0000-0001-8543-741X)

**Robert D. Crapnell** – John Dalton Building, Faculty of Science and Engineering, Manchester Metropolitan University, Manchester M1 5GD, U.K.; [orcid.org/0000-0002-8701-3933](https://orcid.org/0000-0002-8701-3933)

**Thomas J. Cleij** – Sensor Engineering Department, Faculty of Science and Engineering, Maastricht University, Maastricht 6200 MD, The Netherlands; [orcid.org/0000-0003-0172-9330](https://orcid.org/0000-0003-0172-9330)

**Hanne Diliën** – Sensor Engineering Department, Faculty of Science and Engineering, Maastricht University, Maastricht 6200 MD, The Netherlands

**Craig E. Banks** – John Dalton Building, Faculty of Science and Engineering, Manchester Metropolitan University, Manchester M1 5GD, U.K.; [orcid.org/0000-0002-0756-9764](https://orcid.org/0000-0002-0756-9764)

**Kasper Eersels** – Sensor Engineering Department, Faculty of Science and Engineering, Maastricht University, Maastricht 6200 MD, The Netherlands; [orcid.org/0000-0002-0214-1320](https://orcid.org/0000-0002-0214-1320)

**Bart van Grinsven** – Sensor Engineering Department, Faculty of Science and Engineering, Maastricht University, Maastricht 6200 MD, The Netherlands; [orcid.org/0000-0002-6939-0866](https://orcid.org/0000-0002-6939-0866)

Complete contact information is available at:

<https://pubs.acs.org/10.1021/acsomega.4c10473>

## Funding

The study is a part of the project “High-tech sensors for monitoring the release of per- and poly-fluoroalkyl substances (PFAS) from recycled plastics in a circular economy (GPMU/20/063)”, funded by KU Leuven, Belgium, and Maastricht University, The Netherlands, through the Global PhD Partnership. This work was also supported by the European Regional Development Fund of the European Union through the PFAS-Resolve project, funded by the Interreg VIA Meuse-Rhine (NL-DE-BE) program, project number IMR6–00027.

## Notes

The authors declare no competing financial interest.

## ■ REFERENCES

- (1) Renai, L.; Del Bubba, M.; Samanipour, S.; Stafford, R.; Gargano, A. F. G. Development of a Comprehensive Two-Dimensional Liquid Chromatographic Mass Spectrometric Method for the Non-Targeted Identification of Poly- and Perfluoroalkyl Substances in Aqueous Film-Forming Foams. *Anal. Chim. Acta* **2022**, *1232*, No. 340485.
- (2) Gonzalez de Vega, R.; Cameron, A.; Clases, D.; Dodgen, T. M.; Doble, P. A.; Bishop, D. P. Simultaneous Targeted and Non-Targeted Analysis of per- and Polyfluoroalkyl Substances in Environmental Samples by Liquid Chromatography-Ion Mobility-Quadrupole Time of Flight-Mass Spectrometry and Mass Defect Analysis. *J. Chromatogr A* **2021**, *1653*, No. 462423.
- (3) Menger, R. F.; Funk, E.; Henry, C. S.; Borch, T. Sensors for Detecting Per- and Polyfluoroalkyl Substances (PFAS): A Critical Review of Development Challenges, Current Sensors, and Commercialization Obstacles. *Chemical Engineering Journal* **2021**, *417*, No. 129133.
- (4) John, J.; Coulon, F.; Chellam, P. V. Detection and Treatment Strategies of Per- and Polyfluoroalkyl Substances (PFAS): Fate of PFAS through DPSIR Framework Analysis. *Journal of Water Process Engineering* **2022**, *45*, No. 102463.
- (5) Skaggs, C. S.; Logue, B. A. Ultratrace Analysis of Per- and Polyfluoroalkyl Substances in Drinking Water Using Ice Concentration Linked with Extractive Stirrer and High Performance Liquid Chromatography – Tandem Mass Spectrometry. *J. Chromatogr A* **2021**, *1659*, No. 462493.
- (6) Jia, Y.; Qian, J.; Pan, B. Dual-Functionalized MIL-101(Cr) for the Selective Enrichment and Ultrasensitive Analysis of Trace Per- and Poly-Fluoroalkyl Substances. *Anal. Chem.* **2021**, *93* (32), 11116–11122.
- (7) Hill, N. I.; Becanova, J.; Lohmann, R. A Sensitive Method for the Detection of Legacy and Emerging Per- and Polyfluorinated Alkyl Substances (PFAS) in Dairy Milk. *Anal. Bioanal. Chem.* **2022**, *414*, 1235–1243.

- (8) Casey, J. S.; Jackson, S. R.; Ryan, J.; Newton, S. R. The Use of Gas Chromatography – High Resolution Mass Spectrometry for Suspect Screening and Non-Targeted Analysis of per- and Polyfluoroalkyl Substances. *J. Chromatogr A* **2023**, *1693*, No. 463884.
- (9) Yu, H.; Chen, H.; Fang, B.; Sun, H. Sorptive Removal of Per- and Polyfluoroalkyl Substances from Aqueous Solution: Enhanced Sorption, Challenges and Perspectives. *Sci. Total Environ.* **2023**, *861*, No. 160647.
- (10) Gong, J.; Fang, T.; Peng, D.; Li, A.; Zhang, L. A Highly Sensitive Photoelectrochemical Detection of Perfluorooctanoic Acid with Molecularly Imprinted Polymer-Functionalized Nanoarchitected Hybrid of AgI-BiOI Composite. *Biosens Bioelectron* **2015**, *73*, 256–263.
- (11) Directive (EU) 2020/2184 of the European Parliament and of the Council of 16 December 2020 on the quality of water intended for human consumption (recast). <https://eur-lex.europa.eu/eli/dir/2020/2184/oj>.
- (12) Gogoi, P.; Yao, Y.; Li, Y. C. Understanding PFOS Adsorption on a Pt Electrode for Electrochemical Sensing Applications. *ChemElectroChem* **2023**, *10* (2), No. e202201006.
- (13) Park, J.; Yang, K. A.; Choi, Y.; Choe, J. K. Novel SsDNA Aptamer-Based Fluorescence Sensor for Perfluorooctanoic Acid Detection in Water. *Environ. Int.* **2022**, *158*, No. 107000.
- (14) Cennamo, N.; D'Agostino, G.; Porto, G.; Biasiolo, A.; Perri, C.; Arcadio, F.; Zeni, L. A Molecularly Imprinted Polymer on a Plasmonic Plastic Optical Fiber to Detect Perfluorinated Compounds in Water. *Sensors (Switzerland)* **2018**, *18* (6), 1836.
- (15) Chen, B.; Yang, Z.; Qu, X.; Zheng, S.; Yin, D.; Fu, H. Screening and Discrimination of Perfluoroalkyl Substances in Aqueous Solution Using a Luminescent Metal-Organic Framework Sensor Array. *ACS Appl. Mater. Interfaces* **2021**, *13* (40), 47706–47716.
- (16) Ahmadi Tabar, F.; Lowdon, J. W.; Bakhshi Sichani, S.; Khorshid, M.; Cleij, T. J.; Diliën, H.; Eersels, K.; Wagner, P.; van Grinsven, B. An Overview on Recent Advances in Biomimetic Sensors for the Detection of Perfluoroalkyl Substances. *Sensors* **2023**, *24* (1), No. s24010130.
- (17) Harrison, E. E.; Waters, M. L. Detection and Differentiation of Per- and Polyfluoroalkyl Substances (PFAS) in Water Using a Fluorescent Imprint-and-Report Sensor Array. *Chem. Sci.* **2023**, *14* (4), 928–936.
- (18) Law, C. S.; Wang, J.; Gunenthiran, S.; Lim, S. Y.; Abell, A. D.; Ahrens, L.; Kumeria, T.; Santos, A.; Voelcker, N. H. Real-Time Detection of per-Fluoroalkyl Substance (PFAS) Self-Assembled Monolayers in Nanoporous Interferometers. *Sens. Actuators, B* **2022**, *355*, No. 131340.
- (19) Garg, S.; Kumar, P.; Greene, G. W.; Mishra, V.; Avisar, D.; Sharma, R. S.; Dumée, L. F. Nano-Enabled Sensing of per-/Poly-Fluoroalkyl Substances (PFAS) from Aqueous Systems – A Review. *J. Environ. Manage* **2022**, *308*, No. 114655.
- (20) Trinh, V.; Malloy, C. S.; Durkin, T. J.; Gadh, A.; Savagatrup, S. Detection of PFAS and Fluorinated Surfactants Using Differential Behaviors at Interfaces of Complex Droplets. *ACS Sens* **2022**, *7* (5), 1514–1523.
- (21) Concellón, A.; Castro-Esteban, J.; Swager, T. M. Ultratrace PFAS Detection Using Amplifying Fluorescent Polymers. *J. Am. Chem. Soc.* **2023**, *145* (20), 11420–11430.
- (22) Hasseb, A. A.; Abdel Ghani, N. D. T.; Shehab, O. R.; El Nashar, R. M. Application of Molecularly Imprinted Polymers for Electrochemical Detection of Some Important Biomedical Markers and Pathogens. *Curr. Opin. Electrochem.* **2022**, *31*, No. 100848.
- (23) Randriamahazaka, H.; Ghilane, J. Electrografting and Controlled Surface Functionalization of Carbon Based Surfaces for Electroanalysis. *Electroanalysis* **2016**, *28* (1), 13–26.
- (24) Ayerdurai, V.; Cieplak, M.; Kutner, W. Molecularly Imprinted Polymer-Based Electrochemical Sensors for Food Contaminants Determination. *TrAC - Trends in Analytical Chemistry* **2023**, *158*, No. 116830.
- (25) Pardeshi, S.; Dhodapkar, R. Advances in Fabrication of Molecularly Imprinted Electrochemical Sensors for Detection of Contaminants and Toxicants. *Environ. Res.* **2022**, *212*, No. 113359.
- (26) Vu, O. T.; Nguyen, Q. H.; Nguy Phan, T.; Luong, T. T.; Eersels, K.; Wagner, P.; Truong, L. T. N. Highly Sensitive Molecularly Imprinted Polymer-Based Electrochemical Sensors Enhanced by Gold Nanoparticles for Norfloxacin Detection in Aquaculture Water. *ACS Omega* **2023**, *8*, 2887–2896.
- (27) Chi, H.; Liu, G. Carbon Nanomaterial-Based Molecularly Imprinted Polymer Sensors for Detection of Hazardous Substances in Food: Recent Progress and Future Trends. *Food Chem.* **2023**, *420*, No. 136100.
- (28) Farooq, S.; Nie, J.; Cheng, Y.; Yan, Z.; Li, J.; Bacha, S. A. S.; Mushtaq, A.; Zhang, H. Molecularly Imprinted Polymers' Application in Pesticide Residue Detection. *Analyst* **2018**, *143* (17), 3971–3989.
- (29) Ashley, J.; Shahbazi, M. A.; Kant, K.; Chidambara, V. A.; Wolff, A.; Bang, D. D.; Sun, Y. Molecularly Imprinted Polymers for Sample Preparation and Biosensing in Food Analysis: Progress and Perspectives. *Biosens Bioelectron* **2017**, *91*, 606–615.
- (30) Geerets, B.; Peeters, M.; Grinsven, B.; Bers, K.; De Ceuninck, W.; Wagner, P. Optimizing the Thermal Read-out Technique for MIP-Based Biomimetic Sensors: Towards Nanomolar Detection Limits. *Sensors* **2013**, *13* (7), 9148–9159.
- (31) Lowdon, J. W.; Diliën, H.; van Grinsven, B.; Eersels, K.; Cleij, T. J. Colorimetric Sensing of Amoxicillin Facilitated by Molecularly Imprinted Polymers. *Polymers (Basel)* **2021**, *13* (13), 2221.
- (32) Wang, Z.; Zhang, Z.; Yan, R.; Fu, X.; Wang, G.; Wang, Y.; Li, Z.; Zhang, X.; Hou, J. Facile Fabrication of Snowman-like Magnetic Molecularly Imprinted Polymer Microspheres for Bisphenol A via One-Step Pickering Emulsion Polymerization. *React. Funct. Polym.* **2021**, *164*, No. 104911.
- (33) Zhao, G.; Liu, J.; Liu, M.; Han, X.; Peng, Y.; Tian, X.; Liu, J.; Zhang, S. Synthesis of Molecularly Imprinted Polymer via Emulsion Polymerization for Application in Solanesol Separation. *Applied Sciences (Switzerland)* **2020**, *10* (8), 2868.
- (34) Pardeshi, S.; Singh, S. K. Precipitation Polymerization: A Versatile Tool for Preparing Molecularly Imprinted Polymer Beads for Chromatography Applications. *RSC Adv.* **2016**, *6* (28), 23525–23536.
- (35) Mostafiz, B.; Bigdeli, S. A.; Banan, K.; Afsharara, H.; Hatamabadi, D.; Mousavi, P.; Hussain, C. M.; Keçili, R.; Ghorbani-Bidkoreh, F. Molecularly Imprinted Polymer-Carbon Paste Electrode (MIP-CPE)-Based Sensors for the Sensitive Detection of Organic and Inorganic Environmental Pollutants: A Review. *Trends in Environmental Analytical Chemistry* **2021**, *32*, No. e00144.
- (36) Tarannum, N.; Khatoun, S.; Dzantiev, B. B. Perspective and Application of Molecular Imprinting Approach for Antibiotic Detection in Food and Environmental Samples: A Critical Review. *Food Control* **2020**, *118*, No. 107381.
- (37) Tasfaout, A.; Ibrahim, F.; Morrin, A.; Brisset, H.; Sorrentino, I.; Nanteuil, C.; Laffite, G.; Nicholls, I. A.; Regan, F.; Branger, C. Molecularly Imprinted Polymers for Per- and Polyfluoroalkyl Substances Enrichment and Detection. *Talanta* **2023**, *258*, No. 124434.
- (38) Rahman, S.; Bozal-Palabiyik, B.; Unal, D. N.; Erkmen, C.; Siddiq, M.; Shah, A.; Uslu, B. Molecularly Imprinted Polymers (MIPs) Combined with Nanomaterials as Electrochemical Sensing Applications for Environmental Pollutants. *Trends in Environmental Analytical Chemistry* **2022**, *36*, No. e00176.
- (39) Selvolini, G.; Marrazza, G. MIP-Based Sensors: Promising New Tools for Cancer Biomarker Determination. *Sensors (Switzerland)* **2017**, *17* (4), 718.
- (40) Cui, F.; Zhou, Z.; Zhou, H. S. Molecularly Imprinted Polymers and Surface Imprinted Polymers Based Electrochemical Biosensor for Infectious Diseases. *Sensors (Switzerland)* **2020**, *20* (4), 996.
- (41) Wilkerson, E. C.; Singampalli, K. L.; Li, J.; Dixit, D. D.; Jiang, X.; Gonzalez, D. H.; Lillehoj, P. B. Affinity-Based Electrochemical Sensors for Biomolecular Detection in Whole Blood. *Anal Bioanal Chem.* **2023**, *415* (18), 3983–4002.
- (42) FitzGerald, L. I.; Olorunyomi, J. F.; Singh, R.; Doherty, C. M. Towards Solving the PFAS Problem: The Potential Role of Metal-Organic Frameworks. *ChemSusChem* **2022**, *15* (19), No. e202201136.

- (43) Kukralova, K.; Miliutina, E.; Guselnikova, O.; Burtsev, V.; Hrbek, T.; Svorcik, V.; Lyutakov, O. Dual-Mode Electrochemical and SERS Detection of PFAS Using Functional Porous Substrate. *Chemosphere* **2024**, *364*, No. 143149.
- (44) Rezaei, M.; Ghanavati, M.; Mohammadi, N.; Khani, S.; Nasirimoghdam, S.; Smiley, E.; Basiryamhabadi, A. A New Sensitive Layer Based on Clcinated Zn/Ti-MOF/Magnetic Molecularly Imprinted Polypyrrole: Application to Preconcentration and Electrochemical Determination of Perfluorooctane Sulfonic Acid by Magnetic Carbon Paste Electrode. *Talanta* **2024**, *276*, No. 126229.
- (45) Lu, D.; Zhu, D. Z.; Gan, H.; Yao, Z.; Luo, J.; Yu, S.; Kurup, P. An Ultra-Sensitive Molecularly Imprinted Polymer (MIP) and Gold Nanostars (AuNS) Modified Voltammetric Sensor for Facile Detection of Perfluorooctane Sulfonate (PFOS) in Drinking Water. *Sens Actuators B Chem.* **2022**, *352*, No. 131055.
- (46) Suhaimi, N. F.; Baharin, S. N. A.; Jamion, N. A.; Mohd Zain, Z.; Sambasevam, K. P. Polyaniline-Chitosan Modified on Screen-Printed Carbon Electrode for the Electrochemical Detection of Perfluorooctanoic Acid. *Microchemical Journal* **2023**, *188*, No. 108502.
- (47) Pierpaoli, M.; Szopińska, M.; Olejnik, A.; Ryl, J.; Fudala-Ksiażek, S.; Luczkiewicz, A.; Bogdanowicz, R. Engineering Boron and Nitrogen Codoped Carbon Nanoarchitectures to Tailor Molecularly Imprinted Polymers for PFOS Determination. *J. Hazard Mater.* **2023**, *458*, No. 131873.
- (48) Korekar, G.; Kumar, A.; Ugale, C. Occurrence, Fate, Persistence and Remediation of Caffeine: A Review. *Environmental Science and Pollution Research* **2020**, *27* (28), 34715–34733.
- (49) Valcárcel, Y.; González Alonso, S.; Rodríguez-Gil, J. L.; Gil, A.; Catalá, M. Detection of Pharmaceutically Active Compounds in the Rivers and Tap Water of the Madrid Region (Spain) and Potential Ecotoxicological Risk. *Chemosphere* **2011**, *84* (10), 1336–1348.
- (50) Karimian, N.; Stortini, A. M.; Moretto, L. M.; Costantino, C.; Bogialli, S.; Ugo, P. Electrochemosensor for Trace Analysis of Perfluorooctanesulfonate in Water Based on a Molecularly Imprinted Poly(o-Phenylenediamine) Polymer. *ACS Sens* **2018**, *3* (7), 1291–1298.
- (51) Clark, R. B.; Dick, J. E. Electrochemical Sensing of Perfluorooctanesulfonate (PFOS) Using Ambient Oxygen in River Water. *ACS Sens* **2020**, *5* (11), 3591–3598.
- (52) Cheng, Y. H.; Barpaga, D.; Soltis, J. A.; Shutthanandan, V.; Kargupta, R.; Han, K. S.; McGrail, B. P.; Motkuri, R. K.; Basuray, S.; Chatterjee, S. Metal-Organic Framework-Based Microfluidic Impedance Sensor Platform for Ultrasensitive Detection of Perfluorooctanesulfonate. *ACS Appl. Mater. Interfaces* **2020**, *12* (9), 10503–10514.
- (53) Mashkoor, F.; Mashkoor, R.; Shoeb, M.; Anwer, A. H.; Jeong, H.; Jeong, C. Freestanding WS<sub>2</sub>-MWCNT Nanocomposite for Electrochemical Detection of Contaminants of Emerging Concern—Perfluorooctanoic Acid “A Forever Chemical” and Supercapacitor Applications. *ACS Sustain. Chem. Eng.* **2023**, *11* (36), 13306–13319.
- (54) Tian, Q.; Chen, S.; Shi, M.; Gao, T.; Zhang, M.; Liao, C.; Li, X.; Dong, Q.; Wang, C. Fluorine-Functionalized MOF Modified GCE for Highly Sensitive Electrochemical Detection of Persistent Pollutant Perfluorooctanoic Acid. *Sens Actuators B Chem.* **2024**, *404*, No. 135309.
- (55) Tabar, F. A.; Lowdon, J. W.; Caldara, M.; Cleij, T. J.; Wagner, P.; Diliën, H.; Eersels, K.; van Grinsven, B. Thermal Determination of Perfluoroalkyl Substances in Environmental Samples Employing a Molecularly Imprinted Polyacrylamide as a Receptor Layer. *Environ. Technol. Innov.* **2023**, *29*, No. 103021.
- (56) Caldara, M.; Lowdon, J. W.; van Wissen, G.; Ferrari, A. G. M.; Crapnell, R. D.; Cleij, T. J.; Diliën, H.; Banks, C. E.; Eersels, K.; van Grinsven, B. Dipstick Sensor Based on Molecularly Imprinted Polymer-Coated Screen-Printed Electrodes for the Single-Shot Detection of Glucose in Urine Samples—From Fundamental Study toward Point-of-Care Application. *Adv. Mater. Interfaces* **2023**, *10* (18), No. 2300182.
- (57) Roberto de Oliveira, P.; Crapnell, R. D.; Garcia-Miranda Ferrari, A.; Wuamprakhon, P.; Hurst, N. J.; Dempsey-Hibbert, N. C.; Sawangphruk, M.; Janegitz, B. C.; Banks, C. E. Low-Cost, Facile Droplet Modification of Screen-Printed Arrays for Internally Validated Electrochemical Detection of Serum Procalcitonin. *Biosens. Bioelectron.* **2023**, *228*, No. 115220.